RSC Advances

This is an *Accepted Manuscript*, which has been through the Royal Society of Chemistry peer review process and has been accepted for publication.

Accepted Manuscripts are published online shortly after acceptance, before technical editing, formatting and proof reading. Using this free service, authors can make their results available to the community, in citable form, before we publish the edited article. This *Accepted Manuscript* will be replaced by the edited, formatted and paginated article as soon as this is available.

You can find more information about *Accepted Manuscripts* in the Information for Authors.

Please note that technical editing may introduce minor changes to the text and/or graphics, which may alter content. The journal's standard Terms & Conditions and the Ethical guidelines still apply. In no event shall the Royal Society of Chemistry be held responsible for any errors or omissions in this *Accepted Manuscript* or any consequences arising from the use of any information it contains.

ROYAL SOCIETY OF CHEMISTRY

www.rsc.org/advances

Functional properties of $ZnCo_2O_4$ nano-particles obtained by thermal decomposition of binary metal nitrate solution

C. R. Mariappan[*,1], R. Kumar[1], G. Vijaya Prakash[2]

[1]Department of Physics, National Institute of Technology, Kurukshetra, Haryana – 136 119, India

[2]Nanophotonics Laboratory, Department of Physics, Indian Institute of Technology-Delhi, New Delhi – 110016, India

Abstract

Spinel-type $ZnCo_2O_4$ nano-crystalline particles are prepared by direct thermal decomposition of solution of binary metal nitrates at relatively low temperatures (100 ^oC). The structural studies from X-ray diffraction and X-ray photoelectron spectroscopy reveal the predominant spinel crystal phase for $ZnCo_2O_4$. The high resolution transmission electron microscopy images with selected area diffraction patterns show the spinal-type $ZnCo_2O_4$ nano-particles have a mean particle size of around 20 nm. The magnetic measurement reveals the weak ferromagnetic properties for the spinel-type $ZnCo_2O_4$ nano-particles. The impedance spectroscopy measurement suggests the p-type nature of prepared $ZnCo_2O_4$ nano-particles. Activation energies in Ar, air and O_2 atmospheric conditions are found to be 0.46 eV, 0.43 eV and 0.35 eV respectively for the temperature below 200 ^oC. For temperatures greater than 200 ^oC, these samples show intrinsic nature with activation energy of 0.57 eV for all atmospheric conditions. The $ZnCo_2O_4$ nano-crystals show the promising chemisorption process related gas sensing behaviour for liquefied petroleum gas and they are investigated by DC and AC impedance measurements. A mechanism for the gas sensing behaviour of $ZnCo_2O_4$ is discussed.

Keywords: Nanoparticles, spinel-structure, optical properties, electrical properties, magnetic properties, gas sensing behaviours.

* Corresponding author: e-mail: crmari2005@yahoo.com

Tel.: +91–1744–233-498; fax: +91-1744–238-050

RSC Advances Accepted Manuscript

1. Introduction

The nano-structured semiconducting $ZnCo_2O_4$ spinel-type oxides have been investigated intensively for various potential applications.[1-8] In addition to the different applications, the attention towards cobalt based spinel-type $ZnCo_2O_4$ is increased very recently due to their p-type semiconducting behavior as a hole transport layer in organic photovoltaics (PVs).[5] The p-type semiconducting oxides with high electrical conductivity, large work function and low synthesis/processing temperatures could be viable interest as p-type electrodes in PVs. During such quest, wide varieties of fabrication techniques have been developed, such as co-precipitation, sol-gel, combustion, micro-emulsion, hydrothermal, molten salt and Pechini polymerization methods are few to mention.[3, 7-11] The major benefit of solution-based synthetic protocol is the molecular level mixing of metal ions which assists the construction of polycrystalline homogeneous nano-structures with enhanced physiochemical properties.

Recently the $ZnCo_2O_4$ nano-structured materials are investigated as chemical gas sensor for hazardous gases such as SO_2, CO, Cl_2, NO_2, CH_3COOH, C_2H_5OH and LPG.[7,10] It is fairly known that gas sensing mechanism of semiconductor metal oxides is mainly surface-controlled and the sensing behaviour is controlled by the transport properties of grain sizes and grain boundaries.[12] Therefore the study of transport properties, their surface morphology dependence and gas/solid interactions have to be investigated for understanding the gas sensing mechanism from nano-granular based devices. However, majority of the gas sensing studies of $ZnCo_2O_4$ are based on bulk measurements such as DC resistance and hardly any reports are available on the effect of dynamically variable electrical quantities such as impedance and capacitance. Impedance spectroscopic method is an unique tool to study the nature of conduction processes and the mechanism of gas/solid interactions, which exploits the molecular dynamic relaxation processes involved during electrical injection.[13-15]

Most of the ultrafine powder or nano-structured $ZnCo_2O_4$ materials are obtained by heating the precursors between 280 ^oC to 600 ^oC.[1-9] The focus of the present article is to propose a simple, inexpensive and effective synthesis of spinel-type $ZnCo_2O_4$ nano-particles by direct thermal decomposition of binary metal nitrate solutions at relatively low temperatures (100 ^oC) and to investigate the functional properties of $ZnCo_2O_4$ nano-particles. Structural and optical properties of the samples are studied utilising thermogravimetric and differential thermal analyses (TG-DTA), powder X-ray diffraction (XRD), Fourier transformation infrared spectroscopy (FTIR), UV-Visible (UV) absorption, Photoluminescence (PL), X-ray photoelectron spectroscopy (XPS), Scanning electron

RSC Advances Accepted Manuscript

microscopy (SEM) and high resolution transmission electron microscopy (HR-TEM) with selected area electron diffraction (SAED) pattern techniques. Magnetic behaviour is studied by vibrating sample magnetometer (VSM) measurement. Electrical properties and gas sensing behaviours are investigated by DC resistance and AC impedance measurement techniques at different temperatures.

2. Experimental

To obtain the $ZnCo_2O_4$ nano-particles, $Zn(NO_3)_2 \cdot 6H_2O$ (1.203g) powder are dissolved in ethanol (10 mL) and stirred for approximately 10 min to obtain a colorless solution. To the resulting solution, ethanoloic solution of $Co(NO_3)_2 \cdot 6H_2O$ (2.355g in 15 mL) has been added drop wise and rapidly stirred for more than six hours at room temperature (RT) to yield a deep purple colored solution. Then the solution was slowly heated to 40 ^oC, 60 ^oC, and 80 ^oC for 2h at each temperature step with stirring. Later, the homogenous solution is allowed to dry at 100 ^oC for 2h to obtain black shiny powder. The obtained powders are calcinated at various temperatures between 200 ^oC to 850 ^oC for 2h further structural characterization.

Structural features are investigated by powder X-ray powder diffraction (XRD; Cu K_α radiation; λ =1.541 Å) using Siemens model-D500 X-ray diffractometer. Thermogravimetric and differential thermal analyses (TG-DTA) are performed for the sample using TA instruments model SDT 2960. The temperature was varied from room temperature to 1000 ^oC at a sweep heating rate of 5 ^oC/min in air. Fourier transform infrared spectra are recorded in the range of 4000-400 cm^{-1} using KBr pellet technique from Shimadzu FTIR-8700 spectrophotometer. For the UV-visible absorbance measurements, the ethanolic solutions of powders are prepared by ultrasonication. The UV-visible absorption and photoluminescence (PL spectra are recorded using Shimadzu UV-2600 absorption spectrophotometer and Shimadzu-2250 photoluminescence spectrometers respectively. The particle size and crystallite of calcined powders are obtained from high resolution transmission electron microscopic (HR-TEM) images and selected area electron diffraction (SAED) pattern with Jeol, (JEM 2100) electron microscope. Surface analysis of the pellet sample are carried out with X-ray photoelectron spectroscopy (XPS, SPECS) using monochromated Al K_α (1486.6 eV) radiation as an excitation source. The core level binding energy values are charge-corrected to the C 1s signal (284.6 eV).

RSC Advances Accepted Manuscript

The nano-crystalline $ZnCo_2O_4$ powders are coaxially pressed into pellet and subjected to fire at 750 ^oC for 10h. In order to confirm the nano-structure of the sintered pellet, the scanning electron microscopy (SEM) investigations were conducted on the cross section of the broken pellet using a JEOL Field Emission SEM model JSM-7500F. For impedance measurements, gold contacts on both faces of the sintered pellet are sputtered using a vacuum coater model BC 300. The impedance measurements are carried on Solartron, Model SI 1260, ac impedance analyzer over the frequency range 1 MHz– 10 Hz at temperature between 50 ^oC to 400 ^oC with different controlled conditions such as air, argon and oxygen. For gas sensing studies, the pellet was housed in a home-made glass container of 750 ml capacity and provided with sample injection port, air inlet and air outlet at different temperatures.

3. Results and Discussion:

Figure 1a shows the XRD patterns of nano-crystalline $ZnCo_2O_4$ powder samples calcinated at different temperatures. All the recorded XRD patterns are in good agreement with the reported diffraction pattern of crystalline $ZnCo_2O_4$ (JCPDS #23-1390), suggesting the phase pure spinel structure contains and no secondary phases even up to 750 ^oC calcination. The cell parameter (a = 8.0989 Å) estimated from XRD pattern at 100 ^oC is in good agreement with literature value of $ZnCo_2O_4$ nano-crystals obtained by combustion synthesis.[9] Also it is comparable with the cell parameter (a = 8.093 Å) of Co_3O_4 powders obtained by molten salt method.[16] The cell parameter of $ZnCo_2O_4$ nano-crystals found to be independent of calcination temperatures. Increasing the calcination temperature up to 850 ^oC leads to traces of secondary phases (Fig 1a). At 850^oC, the substitution of Zn^{2+} by Co^{2+} is more favourable due to their similarity of ionic charge and radii, leading to formation of ZnO and Co_3O_4 secondary phases. The substitution of Zn^{2+} by Co^{2+} ions does not lead to a deformation in the measurable XRD pattern of the spinel Co_3O_4 due to comparable cell parameter with $ZnCo_2O_4$. Average crystallite size was calculated by using Williamson-Hall analysis, which takes both the mean crystallite size D and strain ε effects into account:[17]

$$\beta^2 = \left(\frac{0.89\lambda}{D\cos(\theta)}\right)^2 + \left(4\varepsilon tan(\theta)\right)^2 + (\beta_0)^2 \qquad (1)$$

where, β is the full width at half maximum (FWHM) of the XRD peak, θ is the angle and β_0 is the instrumental broadening. Mean crystallite size of $ZnCo_2O_4$ increases from 20 nm (100 ^oC) to 55 nm (750 ^oC) with calcined temperatures.

RSC Advances Accepted Manuscript

TG-DTA measurements depicted in Fig. 1b show the thermal evolution in air for as prepared sample. The TG curve shows three weight losses, the initial loss (~3%), up to 150 ^{o}C, is due to the evaporation of moisture or hydrated water. The second loss between 230 ^{o}C and 350 ^{o}C is most likely due to the evaporation of excess native nitrate moieties. Finally, the third weight loss (~5%) accompanied by an endothermic peak around 875 ^{o}C is attributed to the reduction of Co^{3+} state to Co^{2+} state. Absence of any exothermic peak reveals that the spinel-type $ZnCo_2O_4$ nano-crystalline phase was formed during the synthesis (prepared at 100 ^{o}C) only, which is also evident from XRD studies (Fig. 1a).

Figure 1c shows the FT-IR spectra of $ZnCo_2O_4$ nanoparticles. The spectra show two strong absorption bands at 666 cm^{-1} and 570 cm^{-1}. The peak at 666 cm^{-1} is ascribed to the stretching vibration mode of tetrahedrally coordinated metal (M) oxides (M–O) and the band at 570 cm^{-1} can be attributed to the octahedrally coordinated metal ions. This observation further supports the spinal crystal structure nature of fabricated $ZnCo_2O_4$.[2]

The spinel-type $ZnCo_2O_4$ nanoparticles show good absorbance of light from 200 nm to 600 nm, as shown in Fig. 2a. The optical band gap energy, E_g, can be estimated by Tauc plots of expression, $(\alpha h\nu)^n = K(h\nu - E_g)$, where hν is the photo energy, α is the absorption coefficient, *K* is a constant relative to the material, and n is 2 for a direct transition or 1/2 for an indirect transition. The $(\alpha h\nu)^2$ vs hν curve for $ZnCo_2O_4$ nano-particles is shown inset Fig. 2a. The estimated optical band gap energy of $ZnCo_2O_4$ nano-particles is 3.37 eV. Furthermore, there is one more absorption characteristic is observed at lower energy 1.99 eV. This absorption band is ascribed to Co interatomic d-d transitions connected with a trigonal ligand field splitting[18], suggests that some amount of the Co ions is interchanged with the tetrahedrally coordinated Zn ions. The Co ion can exist in this coordination since the ionic radius is similar to Zn ions.[19,20] Photoluminescence spectra of $ZnCo_2O_4$ nano-particles with different excitation wavelengths are depicted in Fig. 2b within the spectra region of 200 nm – 900 nm. For all excitation wavelengths, within the band edge, a single peak is observed at 3.41 eV (365 nm) and it ascribed as near-band edge emission of sample.

In order to establish the nano structure and crystal phase nature of the synthesized $ZnCo_2O_4$, the HR-TEM and SEAD data were recorded and reported in Fig. 3. The TEM images of $ZnCo_2O_4$ powder synthesised at 100 ^{o}C reveal the average particle size of ~ 20 nm (Fig. 3). The SEAD pattern (inset Fig. 3a) of the sample prepared at 100 ^{o}C is clearly displaying the diffraction rings with bright spots indicating the nano-crystalline nature of the

RSC Advances Accepted Manuscript

sample. The diffraction rings are assigned to (111), (220), (311), (400), (511) and (440) planes, which are in good agreement with the XRD results (Fig 1a). The close view HR-TEM images (Fig. 3c, d) depict well developed lattice fringes, which correlate well with the XRD results. The estimated d value is 2.46 Å corresponds to the (311) Miller indices of spinel-type $ZnCo_2O_4$. Figures 3b &d show the TEM and SEAD pattern of sample calcined at 750 ^oC for 2h. The comparative results justify the crystallite size increase with the increase of calcination temperature and generate well-defined shape of the particles with average diameter of ~55 nm. The sizes of crystallites are also in good agreement with the William-Hall XRD analysis estimations. The SEAD patterns (inset of Fig. 3a&b) and close view HR-TEM images (inset of Fig. 3c,&d) of the sample prepared at 100 ^oC and calcined at 750 ^oC showed the similar crystal features. Therefore, it is convenient to conclude that as low as 100 ^oC is found to be an optimum condition for the formation of nano-crystalline $ZnCo_2O_4$ phase.

The surface chemical compositions of $ZnCo_2O_4$ nanoparticle are obtained by XPS analysis. Figure 4a displays a survey spectrum of $ZnCo_2O_4$ nanoparticle calcined at 750 ^oC for 2h and it reveals the characteristic peaks of Zn, Co, O, and C elements. Figure 4b shows two strong peaks at 794.40 eV and 779.34 eV for Co $2p_{1/2}$ and Co $2p_{3/2}$ respectively, confirms the presence of Co in a 3+ oxidation state.[21] High resolution Zn 2p spectrum (Fig. 4c) shows two peaks with binding energy values of 1044.05 eV and 1021.0 eV, assigned to Zn $2p_{1/2}$ and Zn $2p_{3/2}$ represent the presence of Zn in a 2+ oxidation state.[10] The O 1s peaks at 529.33 eV and 531.18 eV correspond to the oxygen species in the spinel structure lattice and the oxygen in hydroxyl species adsorbed on the surface due to the ex situ measurement conditions (Fig. 4d) respectively.[21] Thus XPS results, along with other aforementioned studies, confirm the formation of $ZnCo_2O_4$ nano-particles with normal spinel structure.

Figure 5 depicts the magnetization versus magnetic field (M–H) curve for the $ZnCo_2O_4$ nano-particles calcinated at 750 ^oC for 2h. The fine shape of M–H curve is a characteristic of a weak ferromagnetic behaviour, although the paramagnetic behaviour has been reported for the bulk $ZnCo_2O_4$ ceramic.[22] The coercive field (H_c) and remanent magnetization (M_r) from M-H curve is found to be 0.10 kOe and 0.012 emu/g respectively as shown in the inset Fig. 5. The smaller values of H_c and M_r prove that the $ZnCo_2O_4$ nano-particles possess the weak ferromagnetic behaviours. The magnetization does not saturate for the maximum applied

RSC Advances Accepted Manuscript

magnetic field 12 kOe and it represents the weak ferromagnetic ordering of the spins in the nano-particles which consists of the small magnetic domains with random orientations.

SEM photograph of the fractured surface of the $ZnCo_2O_4$ pellet sintered at 750 ^oC for 10h is shown in Fig. 6. The shape of the grains in the sintered pellet is close to circular and is similar to the TEM result (Fig. 3b). This SEM image also reveals that the grains are well connected which would facilitate conduction pathway for the charge carriers. Also the EDX result shows the atomic ratio of Zn:Co is 1:2.

Complex impedance spectra of nano-crystalline $ZnCo_2O_4$ pellet at different temperatures in air are shown in Figure 7a. A single semi-circle is observed at different temperatures and the diameter of the semicircle is observed to decrease with temperature. Figure 7b shows the Nyquist plots of AC impedance of sample at 150 ^oC with different ambient conditions such as air, Ar and O_2. Based on the measured impedance data, the representative electrical equivalent circuit was established as shown in the inset Fig. 7a. In the equivalent circuit elements, the resistance of the sample is represented as R, the capacitance is denoted as "C" and inductance is represented as L due to cable. The measured impedance data were fit to the equivalent circuit using Zview® software.

The R of the sample decreases with increase in temperature due to increase of the mobility of charge carrier and the number density (N_d), whereas the C of the sample slightly increases with temperature. The fitted capacitance values of nano-crystalline $ZnCo_2O_4$ pellet in presence of air are 39.7 pF at 50 ^oC, 42.5 pF at 100 ^oC, 43.8 pF at 150 ^oC, 45.1 pF at 200 ^oC, 45.9 pF at 250 ^oC and 46.8 pF at 300 ^oC. The chemisorbed oxygen molecules are converted into oxide ions by capturing the free electrons and create the holes on the valence band. It creates the negatively charged layer over the grain and also the positively charged grain interior.[14] This space charge layer is a kind of capacitor, since the electrical charge exists locally at the grain boundary.[23] The relaxation time (τ = RC) of $ZnCo_2O_4$ decreases with temperature due to decreasing of R.

A deeper insight into the electrical properties of the nano-crystalline $ZnCo_2O_4$ pellet was obtained from the spectroscopic plots of electric modulus (M″) and impedance (Z″) versus frequency (ν) at 150 ^oC (Fig. 7c) in air, Ar and O_2 atmosphere conditions. Peak frequency of both the curves (Z″ and M″) is same, which indicate that the impedance peak associated with the RC element is responsible for the modulus peak. The associated capacitances are of the order of pF and it is characteristic of the bulk sample. The maximum of M″ is almost same at 150 ^oC in air, Ar and O_2, whereas the maximum of Z″ is decreased with resistance at 150 ^oC

RSC Advances Accepted Manuscript

in air, Ar and O_2. The relaxation frequency ($\nu=1/2\pi RC$) of $ZnCo_2O_4$ is high in the presence of O_2 compared to in the presence of Ar and air. It reveals that the relaxation process of charge carrier is distorted by the different atmospheric conditions for $ZnCo_2O_4$ nano-crystals.

The DC conductivity σ_{dc} was calculated by multiplying the inverse of resistance (1/R) with the ratio of thickness to area of the sample pellet. The estimated DC conductivity at 150 ^oC (σ_{dc} = 2.85 x 10^{-6} S/cm) of $ZnCo_2O_4$ in the presence of O_2 atmosphere is higher than the values observed in the presence of air (1.45 x 10^{-6} S/cm) and Ar atmosphere (7.88 x 10^{-7} S/cm). It can be speculated that when the partial pressure of O_2 is increased, more number of chemisorbed oxygen molecules can be converted into either O^{2-} or O^- by taping the free electron from the $ZnCo_2O_4$ and creating more holes on the valance band. As result of increasing number of holes charge carriers, the conductivity of sample is enhanced. Overall results suggest that the fabricated $ZnCo_2O_4$ is of p-type, having holes as major charge carriers for the electrical conduction.

Results of the temperature dependence of the DC conductivity $\sigma_{dc}(T)$ in different ambient conditions are shown in Fig. 7d. The $\sigma_{dc}(T)$ plots of nano-crystalline $ZnCo_2O_4$ pellet shows the behavior of similar to that of conventional extrinsic semiconductors. The $\sigma_{dc}(T)$ are separated into two different sections: (I) 50 ^oC - 200 ^oC and (II) 200 ^oC - 400 ^oC. The $\sigma_{dc}(T)$ of $ZnCo_2O_4$ in section I is an extrinsic origin from the acceptor level, while the $\sigma_{dc}(T)$ in section II is of intrinsic origin. The activation energies (E_A) for dc conductivity of $ZnCo_2O_4$ nano-particles are obtained by Arrhenius equation. The estimated activation energy (E_A) of sample is found to be 0.46 eV, 0.43 eV and 0.35 eV for the temperature range of 50 ^oC - 200 ^oC (extrinsic origin) in Ar, air and O_2 atmospheres respectively. A moderate difference in activation energies under various atmospheric conditions is due to existence of different local electrical field or different size of energy barrier locally at the grain boundary. For the temperature range above 200 ^oC (intrinsic origin), the activation energy is observed to be 0.57 eV in all the atmospheric conditions (O_2, Ar and air). It reveals that the energy barrier for electrical conduction is independent of atmospheric conditions above 200 ^oC. The thermal energy $\geq$42 meV is indeed sufficient to reduce/remove the different size of the energy barrier exists locally at grain boundary due to the different ambient. Hymavathi et al have reported the E_A of $ZnCo_2O_4$ bulk ceramic is 1.01 eV for the temperature range of 50 ^oC to 500 ^oC in air.[21] Kim et al have observed the E_A of $ZnCo_2O_4$ thin film is 42 meV for the temperature range of -93 ^oC to 200 ^oC.[22] The activation energy observed for present nano-crystalline

RSC Advances Accepted Manuscript

$ZnCo_2O_4$ pellet is lower than the $ZnCo_2O_4$ bulk ceramic[24] and higher than the $ZnCo_2O_4$ thin film.[25]

The gas sensing behaviour for spinel-type $ZnCo_2O_4$ nano-crystals was studied by dc resistance measurement technique as a function of temperature for 500 ppm of LPG. Most favourable response found at a temperature of 365 ^oC as shown in Fig. 8a. The resistance of the sample increases with LPG. The response and recovery times are defined as the time taken to reach 90% of the final resistance value. The response and recovery time for LPG is found to be 85 (s) and 95 (s) respectively at 365 ^oC. Sensitivity for a given concentration of LPG, was calculated by the ratio of R_g/R_a where R_a is the resistance of the sensor in air and R_g is the resistance of the sensor in presence of the LPG. Gas sensitivity increases with concentration at 365 ^oC as shown in the inset Fig. 8a.

Figure 8b describes the Nyquist plots of AC impedance of $ZnCo_2O_4$ at 365 ^oC in the presence of air and in the presence of 100 ppm of LPG. A single half semi-circle is obtained which increased with analyte gas. In order to understand the changes of resistance and capacitance of sample with LPG, we measured them as function of time at a fixed ac frequency, which was close to the relaxation frequency of the sample ($\nu=1/2\pi R_aC_a$) as shown in Fig. 8c. The gas sensing mechanism belongs to the surface controlled nature, in which the grain size, surface states and the density of chemisorbed oxygen ions play the significant roles.[10] As discussed previously, when the $ZnCo_2O_4$ nano-crystals are exposed to air at elevated temperature, chemisorbed oxygen molecules can capture the free electrons and create the holes on the valence band. It can be described by:

$$O_2\ (gas) \leftrightarrow O_2\ (ads) \quad (2)$$

$$O_2\ (ads) + 4e^- \leftrightarrow 2O^{2-}\ (ads) \quad (3)$$

The stabilization of the surface resistance and capacitance is dependent on the equilibrium of the chemisorptions process (equ. (3)). Such stabilised chemisorbed surface resistance can be changed by any process that disturb the equilibrium. The free electrons are released when the reducing gases (LPG contains CH_4, C_3H_8, C_4H_{10} etc.) are interact with the chemisorbed oxide ions of the $ZnCo_2O_4$ surface. This eventually decreases the holes concentration and consequently results in the increase of resistance. However, the change in the capacitance values is not clearly accounted in the case of LPG sensor (Fig. 8c). Since the capacitance is directly proportional to the dipole moment, relatively smaller values of LPG (μ=0.084 for propane, μ=0 for butane, μ=0.13 for isobutene) hardly any changes are observed. To check

RSC Advances Accepted Manuscript

the cross sensitivity, the AC impedance was measured towards 5000 ppm of H_2 at 365 ^oC as shown in Fig. 8d. Considerable changes on AC impedance or resistance and capacitance were not observed with 5000 ppm of H_2 to $ZnCo_2O_4$.

4. Conclusions

Nano-structured $ZnCo_2O_4$ powders were successfully synthesized at relatively low temperatures (100 ^oC). Present XRD and HR-TEM studies revealed that the $ZnCo_2O_4$ nano-particle exists in phase pure spinel-type structure with cell parameter of a = 8.0989 Å. Average crystallite size is found to be approximately 20 nm for the sample prepared at 100 ^oC. The optical band-gap energy of $ZnCo_2O_4$ nano-particle is found to be 3.37 eV. Magnetic measurements revealed the weak ferromagnetic properties. Activation energies of DC conductivity are found to be 0.46 eV, 0.43 eV and 0.35 eV in Ar, air and O_2 respectively for the temperature range of 50 ^oC – 200 ^oC and 0.57 eV in all atmospheric conditions (Ar, air and O_2) for the temperature region of 220 ^oC – 400 ^oC. Gas sensing characteristics of nano-sized $ZnCo_2O_4$ is examined by dc and ac impedance measurements. Most favourable response was found at a temperature of 365 ^oC towards LPG and the sensitivity is observed to increase with concentration. The changes on the DC resistance/real part of impedance of the sample in the presence of LPG is related to chemisorption processes and governed by the number density of charge carriers.

Acknowledgments

The financial support by SERB-DST (India) research grant No. SERB/F/5418/2014-15 is gratefully acknowledged. We are grateful to A. Sreeramamurthy and P.C. Clinsha for the XPS measurements. We thank profusely Scott E. Harpstrite and Dr. S. Jothilingam, University of St. Louis, USA, Dr. C. R. Ramanathan for critical reading of the manuscript. The work is also partly supported by High-Impact research initiative of IIT Delhi.

RSC Advances Accepted Manuscript

References:

1. M. V. Reddy, G. V. Subba Rao, and B. V. R. Chowdari, *Chem. Rev.,* 2013, **113,** 5364.
2. W. Luo, X. Hu, Y. Sun and Y. Huang, *J. Mater. Chem.,* 2012, **22**, 8916.
3. M.V. Reddy, K.Y.H. Kenrick, T.Y. Wei, G.Y. Chong, G.H. Leong and B.V.R. Chowdari, *J. Electrochem. Soc.,* 2011, **158,** A142.
4. M. Davis, C. Gumeci, B. Black, C. Korzeniewski and L. Hope- Weeks, *RSC Adv.,* 2012, **2,** 2061.
5. N. H. Perry and T. O. Mason, *J. Am. Ceram. Soc.,* 2013, **96**, 966.
6. Y. Qiu, S. Yang, H. Deng, L. Jin and W. Li, *J. Mater. Chem.,* 2010, **20**, 4439.
7. X. Niu, W. Du and W. Du, *Sens. Actuators B,* 2004, **99**, 405.
8. Z. Jia, D. Ren, A. Wang and R. Zhu, *Appl. Surf. Sci.,* 2013, **270,** 312.
9. Y. Sharma, N. Sharma, G.V.S. Rao and B.V.R. Chowdari, *Adv. Funct. Mater.,* 2007, **17**, 2855.
10. S. Vijayanand, P.A. Joy, H.S. Potdar, D. Patil and P. Patil, *Sens. Actuators B,* 2011, **152,** 121.
11. B. Liu, J. Zhang, X. Wang, G. Chen, D. Chen, C. Zhou and G. Shen, *Nano Lett.,* 2012, **12**, 3005.
12. G. Korotcenkov, S.-D. Han, B.K. Cho and V. Brinzari, *Critical Rev. Sol. State Mater. Sci.,* 2009, **34,** 1.
13. Z. Ling, C. Leach and R. Freer, *Sens. Actuators B,* 2002, **87,** 215.
14. C. Malag`u, M.C. Carotta, S. Gherardi, V. Guidi, B. Vendemiati and G. Martinelli, *Sens. Actuators B*, 2005, **108,** 70.
15. A. Labidi, C. Jacolin,M. Bendahan, A. Abdelghani, J. Guerin, K. Aguir and M. Maaref, *Sens. Actuators B,* 2005, **106,** 713.
16. M.V. Reddy, Z. Beichen, L.J. Nicholette, Z. Kaimeng and B.V.R. Chowdari, *Electrochem. Solid State Lett.,* 2011, **14,** A70.
17. G.K. Williamson and W.H. Hall, *Acta Metall.,* 1953, **1,** 22.
18. K. Samanta, P. Bhattacharya, and R. S. Katiyar, *Appl. Phys. Lett.,* 2005, **87,** 101903.
19. R. D. Shannon and C. T. Prewitt, *Acta Crystallogr., Sect. B: Struct. Crystallogr. Cryst. Chem.,* 1969, **25,** 925.
20. M. Dekkers, G. Rijnders and D. H. A. Blank, *Appl. Phys. Lett.,* 2007, **90,** 021903.

RSC Advances Accepted Manuscript

21. B. Varghese, T.C. Hoong, Z. Yanwu, M.V. Reddy, B.V.R. Chowdari, A.T S. Wee, T.B.C. Vincent, C.T. Lim and C.H. Sow, *Adv. Funct. Mater.,* 2007, **17,** 1932.

22. P. Cossee, *Recueil,* 1956, **75,** 1089.

23. M. Labeau, U. Schmatz, G. Delabouglise, J. Roman, M. Vallet-Regi and A. Gaskov, *Sens. Actuators B,* 1995, **26,** 49.

24. B. Hymavathi, B. R. Kumar and T.S. Rao, *AIP Conf. Proc.*, 2012, **1461,** 299.

25. H.J. Kim, I.C. Song, J.H. Sim, H. Kim, D. Kim, Y.E. Ihm and W.K. Choo, *Appl. Phys. Lett.,* 2004, **95,** 7387.

RSC Advances Accepted Manuscript

Figure Captions:

Figure 1. (a) XRD patterns of sample after calcinated at different temperatures for 2h. (b) TG and DTA curves for as synthesized sample at 100 ^{o}C. (c) FTIR spectra of $ZnCo_2O_4$ nano-particles.

Figure 2. (a) UV-Visible absorption spectra for the $ZnCo_2O_4$ nano-particles. The inset shows the $(\alpha h\nu)^2$ versus $h\nu$. (b) PL spectra of $ZnCo_2O_4$ nano-particles at various excitation wavelengths (as indicated in ligand titles).

Figure 3. (a) TEM image for the $ZnCo_2O_4$ nano-particles synthesized at 100 ^{o}C. (b) TEM image for the $ZnCo_2O_4$ nano-particles calcinated at 750 ^{o}C for 2h. The inset shows the corresponding SEAD pattern. (c) High resolution lattice image of $ZnCo_2O_4$ nano-particle synthesized at 100 ^{o}C. (d) High resolution lattice image of $ZnCo_2O_4$ nano-particle calcinated at 750 ^{o}C for 2h.

Figure 4. XPS spectra for the $ZnCo_2O_4$ nano-particles: (a) survey spectra and high-resolution (b) Zn 2p, (c) Co 2p, (d) O 1s spectra.

Figure 5. Magnetization vs. magnetic field (M-H) measured at 26 ^{o}C for $ZnCo_2O_4$ nano-particles.

Figure 6. SEM micrograph with EDX information of the fracture surface of the $ZnCo_2O_4$ nano-crystalline pellet sintered at 750 ^{o}C for 2h.

Figure 7. (a) Complex impedance plots for $ZnCo_2O_4$ at different temperatures. A representative equivalent circuit is shown in the inset figure. (b) Nyquist plots of AC impedance for $ZnCo_2O_4$ at 150 ^{o}C with different ambient conditions (air, Ar and O_2). (c) Impedance (Z'') and Modulus (M'') spectroscopic plots for $ZnCo_2O_4$ at 150 ^{o}C with different ambient conditions (air, Ar and O_2). (d) Temperature dependent dc conductivity of $ZnCo_2O_4$ in air, Ar and O_2 atmosphere.

Figure 8. (a) Typical resistance response characteristics of nanocrystalline $ZnCo_2O_4$ pellet towards 500 ppm analyte gas (LPG) at a sensor operating temperature of 365 ^{o}C. The inset shows the sensitivity (R_g/R_a) as a function of concentration of LPG at 365 ^{o}C. (b) Complex impedance plot of $ZnCo_2O_4$ pellet with and without analyte gas (LPG) at 365 ^{o}C. (c) Real part of impedance (Z') and real part of capacitance (C') responses at 100 kHz towards 500 ppm of LPG at 365 ^{o}C. (d) Complex impedance plot of $ZnCo_2O_4$ with 5000 ppm of H_2 and without H_2 at 365 ^{o}C.

RSC Advances Accepted Manuscript

Figure 1

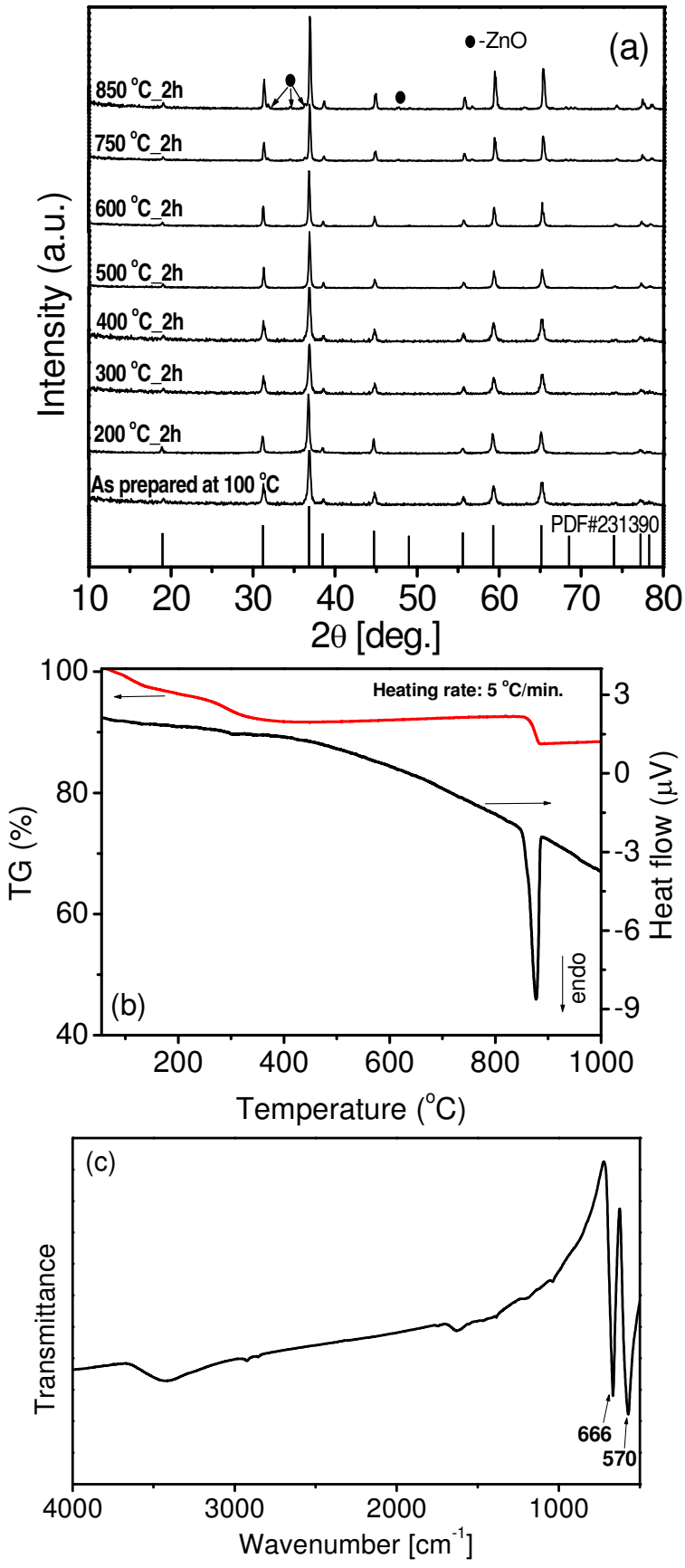

RSC Advances Accepted Manuscript

Figure 2

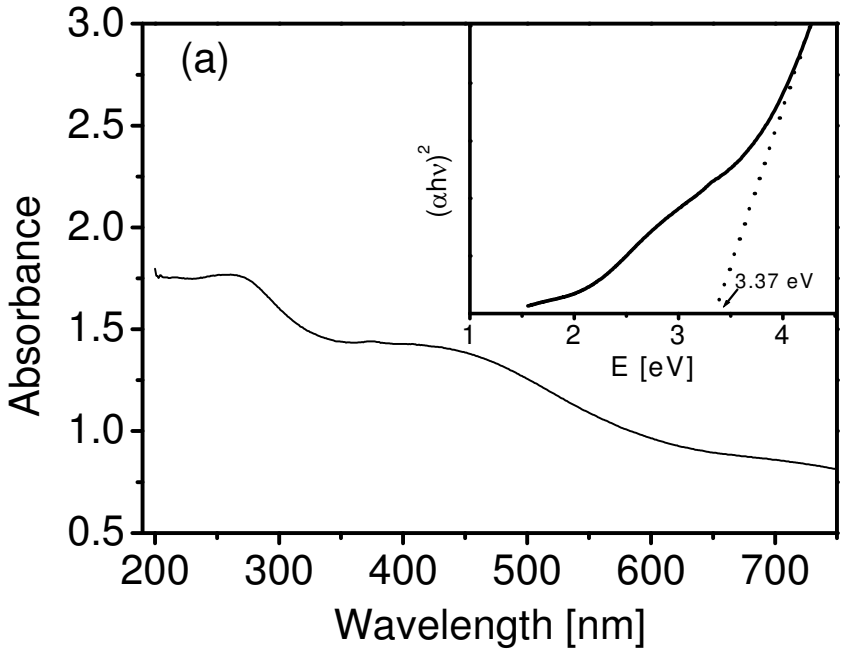

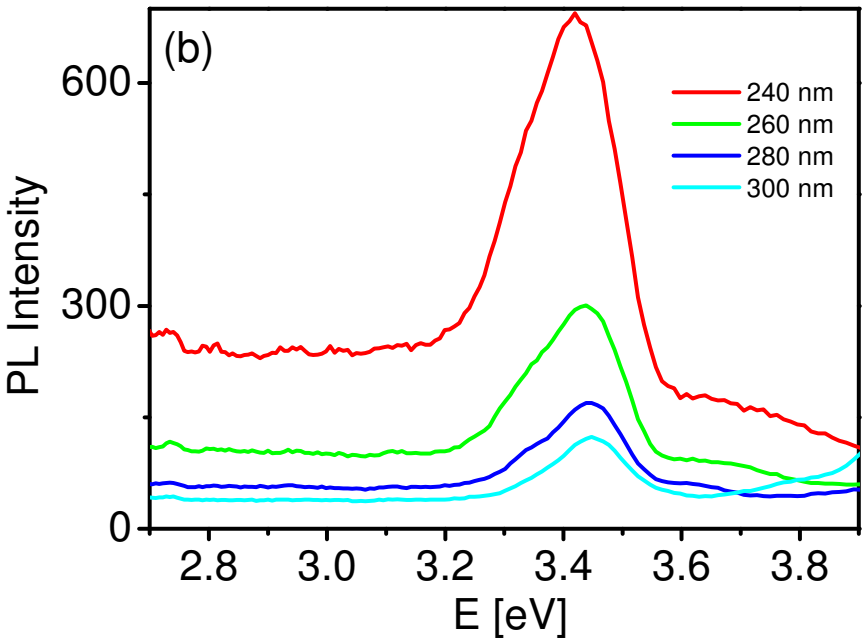

RSC Advances Accepted Manuscript

Figure 3

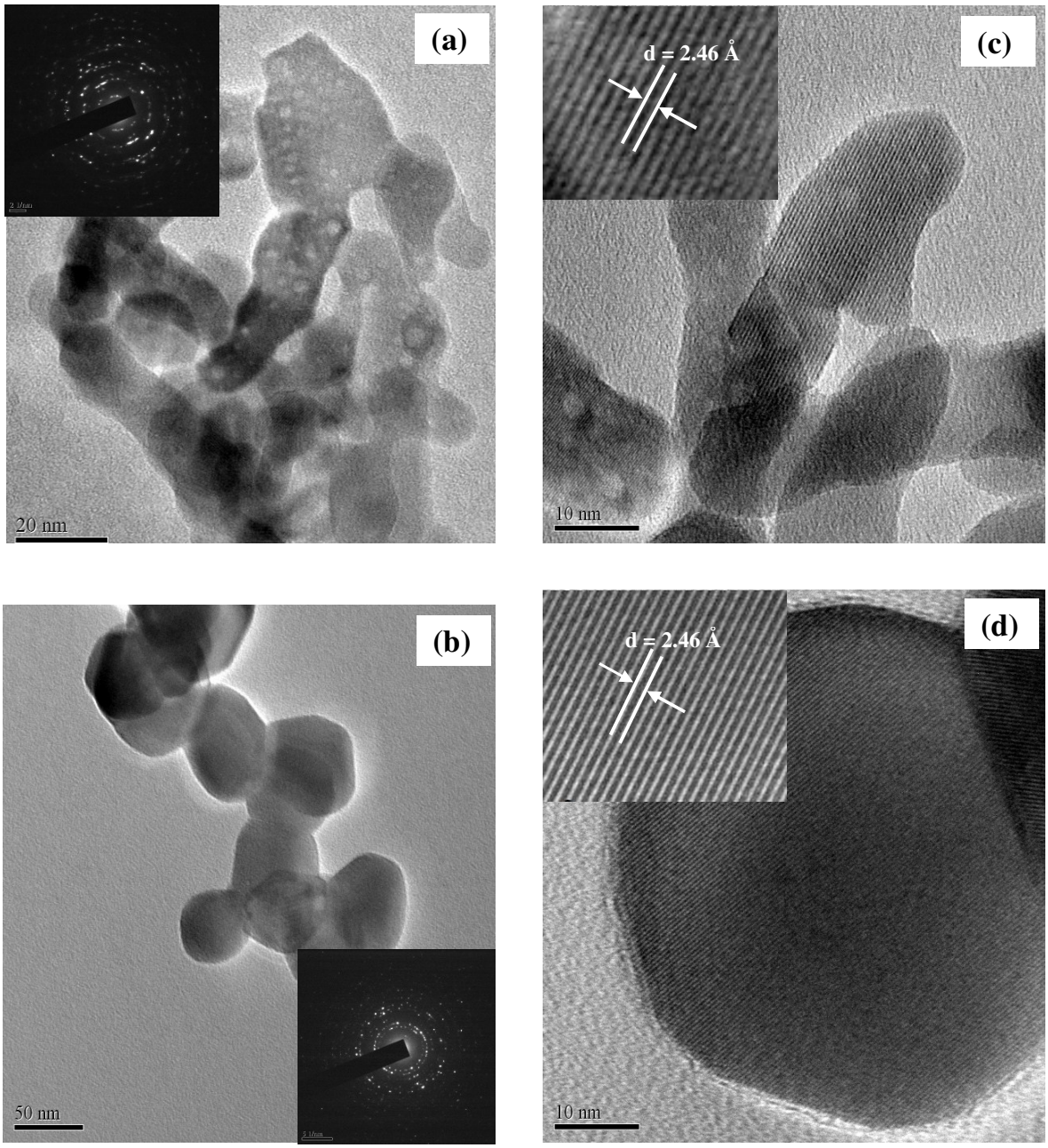

RSC Advances Accepted Manuscript

Figure 4

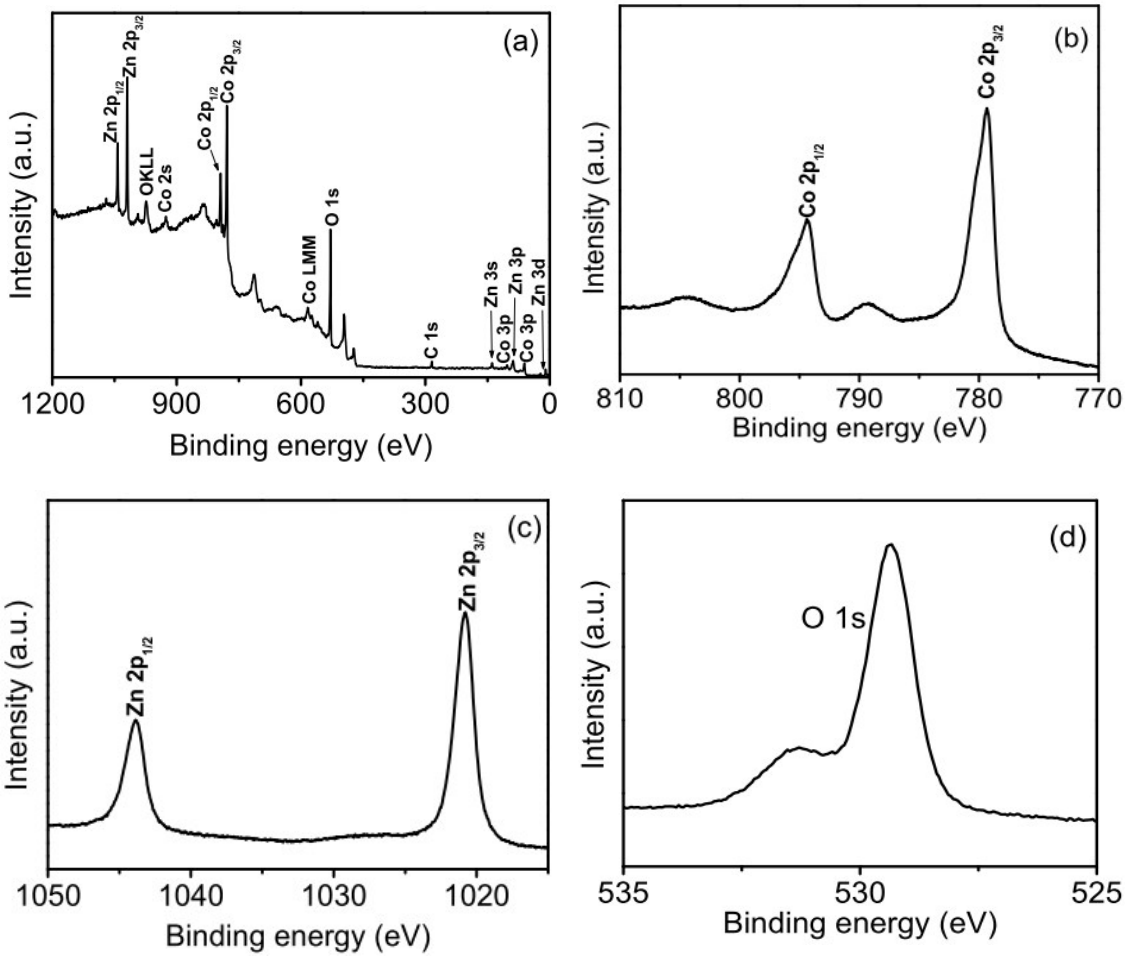

RSC Advances Accepted Manuscript

Figure 5

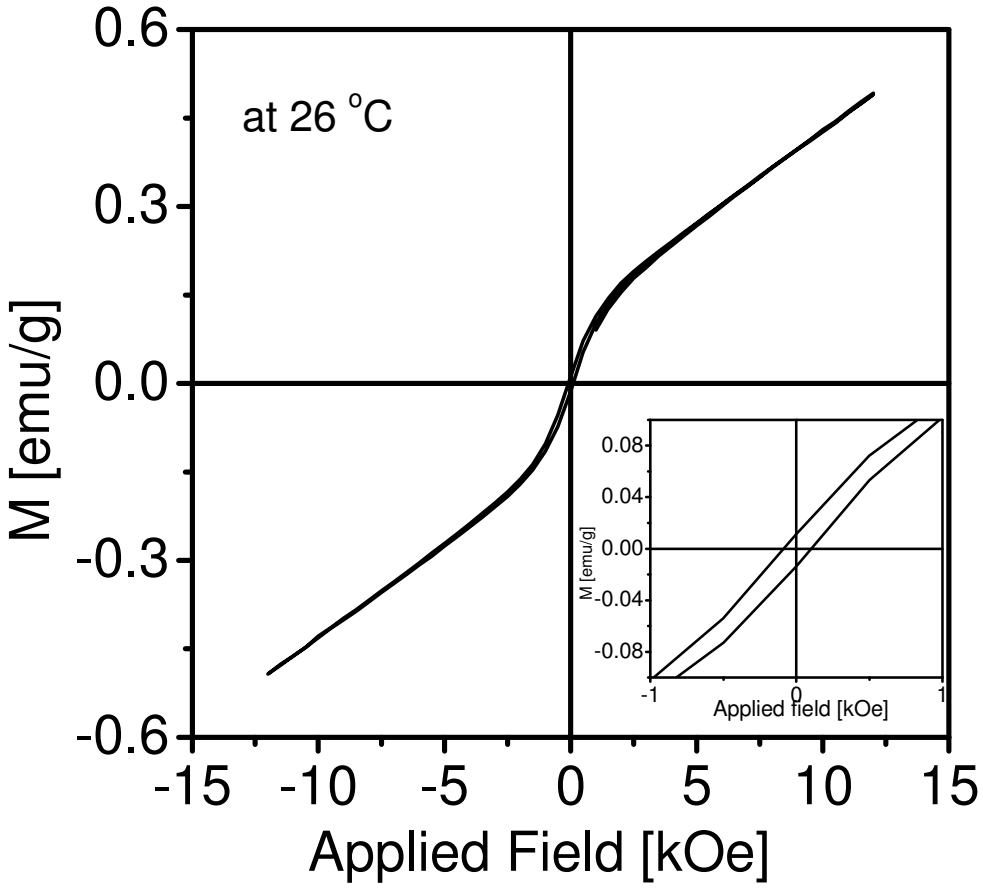

RSC Advances Accepted Manuscript

Figure 6

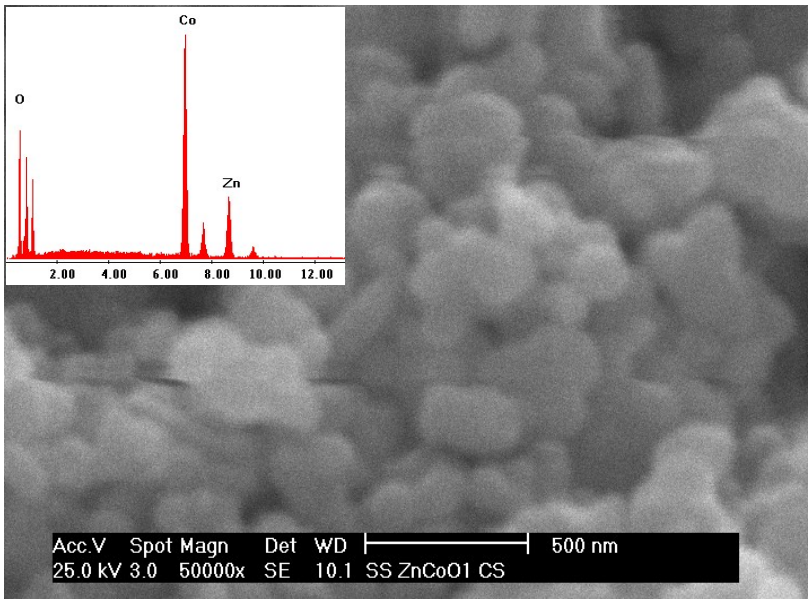

RSC Advances Accepted Manuscript

Figure 7

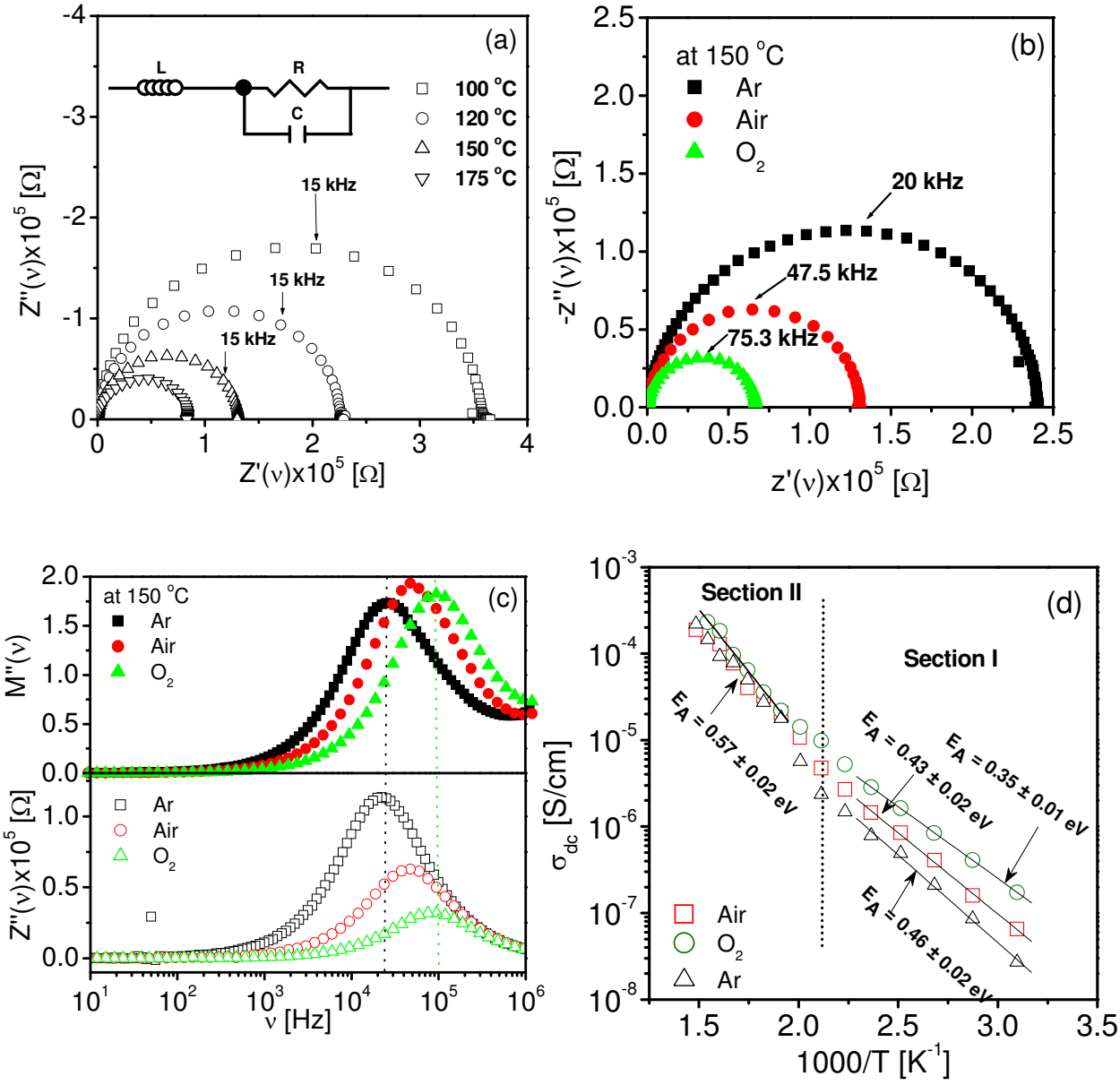

Figure 8

RSC Advances Accepted Manuscript

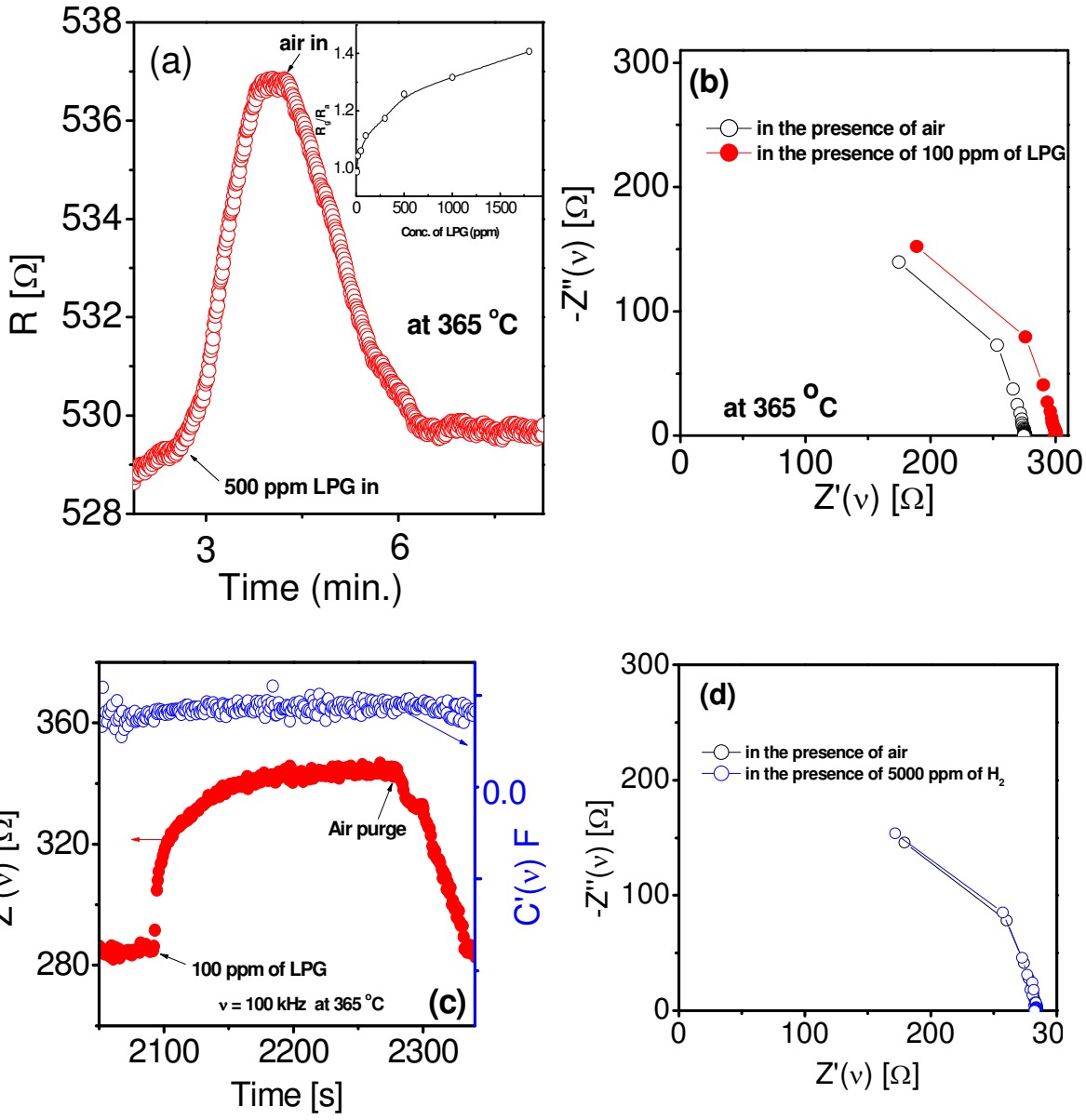

RSC Advances Accepted Manuscript